J Appl Electrochem (2012) 42:679–687
DOI 10.1007/s10800-012-0426-0

ORIGINAL PAPER

On the stability of the flow in multi-channel electrochemical systems

A. Alexiadis · M. P. Dudukovic · P. Ramachandran · A. Cornell

Received: 24 January 2012 / Accepted: 27 April 2012 / Published online: 12 May 2012

Abstract The importance of the fluid dynamics in the modelling of electrochemical systems is often underestimated. The knowledge of the flow velocity pattern in an electrochemical cell, in fact, can allow us to associate certain electrochemical reactions with specific fluid patterns to maximize the yield of some reaction and, conversely, to minimize unwanted or side reactions. The correct evaluation of the convective term in the Nernst–Planck equation, however, requires the solution of the so-called Navier–Stokes equations, and computational fluid dynamics (CFD) is today the established method to numerically solve these equations. In this work, a CFD model is employed to show that the gas–liquid flow pattern can be remarkably different in a single channel or in a multi-channel gas-evolving electrochemical system. In the single channel, in fact, under certain conditions, vortices and recirculation regions can appear in the flow, which does not appear in the multi-channel case. The reason of this difference is found in the uneven distribution of the small bubbles in the two cases. Additionally, a second, simplified, model of the flow is discussed to show how a higher concentration of small bubbles in the single channel system can destabilize the flow.

A. Alexiadis (✉) · A. Cornell
Department of Chemical Engineering and Technology, Applied Electrochemistry, Royal Institute of Technology, KTH, 100 44 Stockholm, Sweden
e-mail: A.Alexiadis@warwick.ac.uk

M. P. Dudukovic · P. Ramachandran
Chemical Reaction Engineering Laboratory (CREL), Department of Energy, Environmental and Chemical Engineering, Washington University, One Brookings Drive, Campus Box 1180, St. Louis, MO 63130, USA

Keywords Chlorate cells · Computational fluid dynamics · Pseudo turbulence · Flow stability

1 Introduction

The study of gas-evolving vertical electrochemical cells is a subject of high importance in electrochemical engineering. However, the majority of the modelling work available in the literature does not focus on describing the evolution and the distribution of gas bubbles or the two phase flow velocity field in the channel between two vertical parallel electrodes. Often, in fact, the velocity profiles are assumed a priori to close the set of equations that describe the mass balance of the various species in the cell (see [1] for a review). Computational fluid dynamics (CFD) is a tool that has already established itself as reliable for simulating the hydrodynamics of various systems of industrial interest, but only lately it has been adopted in electrochemistry (e.g. [2–13]) and, in this study, it is used to calculate the flow in electrochemical systems under different conditions and geometries.

In industrial practice, in fact, electrochemical processes are often carried out in systems that contain a series (generally of the order of hundreds) of parallel channels (gaps) between electrode plates immersed in a large reactor that contains the electrolytes. Electrochemically evolved gas bubbles are produced at the electrodes in the dissolved state; small bubble nucleation starts at the imperfections of the electrode surface and then feeds the surrounding, highly supersaturated, electrolyte [14, 15]. The generated bubbles are responsible for the gas-lift effect that promotes global circulation of the liquid in the cell. They also enhance local mixing which helps in continuously refreshing the

electrolyte in the vicinity of the electrodes. Experiments, however, are often carried out in single channel configurations in the laboratory with the implicit assumption that the observed significant variables will be approximately the same as in all the channels of a larger system subject to maintaining geometric similarity [e.g. 9, 16]. Under circumstances frequently encountered in practice, however, this assumption is not correct [11] and the velocity patterns in the single channel and in the multi-channel configuration can be significantly different. In this work, some of the results of our previous works [10–13] are connected together to provide a detailed theory explaining the differences between these two systems. We apply, in particular, the approach developed in [12] for investigating the flow stability in single channel systems to the CFD data presented in [11] for the case of multi-channel systems.

Intuitively, based on the concepts of natural convection, the chimney effect or the lift involved by gas bubbles, it is not difficult to speculate that the flow and the flow stability is different when it is confined to one channel (where upstream and downstream are interacting in the same channel) or three channels (where part of the return flow is outside the active channel). The main point of this study, however, is related to the quantification of these effects as a function of the gas flux. It must be noted, though, that no coupling between the current density and the flow is assumed. This means that the current density is not influenced by the void fraction as it should be. The reason of this simplification is that, as discussed in Sect. 2, the value of the void fraction at the electrode depends on the particular interaction between the gas phase and the specific electrode (e.g. material and/or surface roughness). The simplification adopted here, therefore, consents, at the expense of the overall accuracy of the model, a more general view not specifically related to any particular electrode.

Investigation concerning the hydrodynamics of other electrochemical systems (e.g. packed-bed electrodes [17], fluorine electrolyser [18, 19], flow-through electrolytic reactors [20] or rotating disc electrode [21–23]), geometric (e.g. [24] larger channel distance) or flow conditions (e.g. turbulent flow [25]) are also available in the literature.

2 Modelling

The calculations in this work refer to electrochemical cells with gas evolution on either the anode or the cathode, as is the case in the chlorate process. We investigated two geometric configurations, the single channel (Fig. 1a) and the multi-channel (three-channel) systems (Fig. 1b). In both cases, the thickness of the gaps is h, their length is L and the length of the upper part is A. As Fig. 1 shows, however, the region A is placed differently in the two geometries (the numerical value, nevertheless, remains the same). In the case of the multi-channel system, there is an additional region with length B at the bottom, which is not present in the single channel geometry. Various configurations with different A, B, h and L have been studied [10–13], but here only results with $A = 20$ mm, $B = 10$ mm, $h = 2$–4 mm and $L = 90$ mm are discussed. The velocity field in both systems is computed by solving the continuity and Navier–Stokes equations for a biphasic flow consisting of a dispersed (gas bubbles) and continuous (liquid) phase according to the so-called Euler–Euler model. The fluid is assumed incompressible and Newtonian and the flow field two-dimensional. Temperature and all the physical properties of the channel material and fluid are considered constant. Since the bubble diameter is small ($d = 0.1$–0.01 mm), the bubbles can be treated as solid spherical particles and their size can be considered approximately constant. All these hypotheses have been previously discussed in detail and justified [10–13]. The assumption of constant diameter, for instance, is reasonably accurate for the case of chlorate cells, where experimental data suggest that coalescence is partially suppressed [16]. In the system under consideration, hydrogen is produced at the cathode according to the reaction:

$$2H_2O + 2e^- \rightarrow H_2 + 2OH^-. \quad (1)$$

Oxygen or any other gas production at the anode is ignored. The volume of O_2 produced in chlorate processes, for instance, is considerably smaller (2–4 %) than that of H_2, while the chlorine produced reacts rapidly with water and is not noticeable as bubbles [16]. The multi-channel system investigated in this study generates gas only from the left side of the central electrode. This situation, of course, does not reflect reality since in industrial configurations all the electrodes produce gas. We chose this option, however, because, in this way, a more direct comparison with the single channel is possible. In general, when certain simplifications in the geometry or in the model were possible, we always chose the option that would reduce the difference between the flow patterns in the two geometries. In this way, we have more confidence that the observed differences between in the computed flow patterns are real (see [11] for details).

The resulting Navier–Stokes equations (see Appendix) are solved numerically. The OpenFOAM® (Open Field Operation and Manipulation) CFD Toolbox was used for this task. Special boundary conditions must be used at the cathode. The gas production at the electrode is determined directly by the following equation:

$$j_{\text{gas}} = \frac{i\text{M}}{z\text{F}\rho_{\text{g}}} = \alpha_{\text{E}} u_{\text{E}}. \quad (2)$$

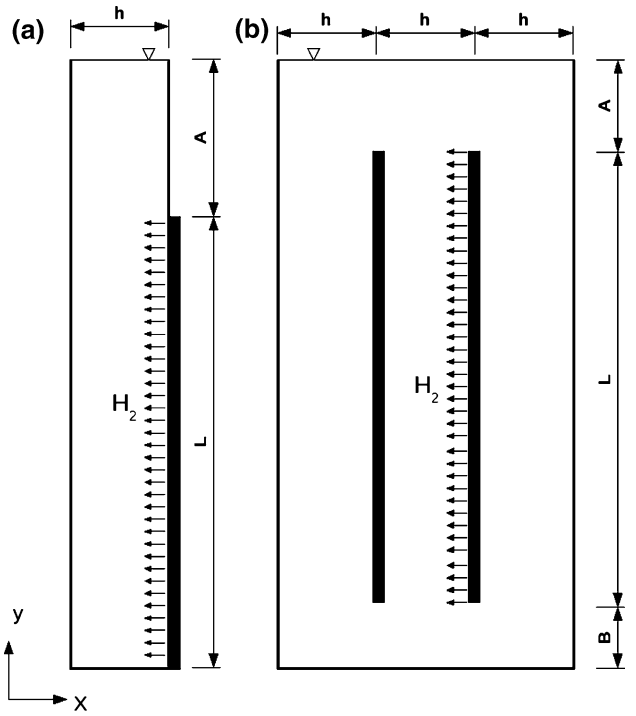

Fig. 1 Single- and multi-channel configurations (figure not in scale)

The values of α_E (void fraction) and u_E (gas velocity at the cathode) must be specified separately at cathode's boundary conditions, but only their product j_{gas} is known from the Faraday's law. It is not completely clear how to assign the values of α_E and u_E since many of the phenomena occurring very close to the electrode are still not completely known. There are different ways to take into account bubble nucleation [26–29], but they are mostly related to the ionic concentrations or the current density distribution at an electrode surface, which are not considered here. In [10], we showed that, under certain conditions (also discussed in [13]), the actual values of α_E and u_E are not fundamental since, provided the same j_{gas}, the differences in void fraction or fluid velocity in the channel concern only a very small region ($\sim$0.03 mm) near the cathode. The top, in both the single- and multi-channel systems is a liquid free surface, which means that the liquid velocity component normal to the surface is zero, while the tangential component has zero gradient. The same boundary, for the gas velocity, is a zero gradient opening, which means that the gas is free to discharge from the liquid surface. It must be stressed, however, that in the multi-channel case the top is considerably larger because located above the common region, which connects the three gaps. This circumstance is fundamental because it is probably the main reason for the difference in flow between the two systems, as discussed in Sect. 3. Concerning the bottom, in both cases, it is simply a wall. The liquid is confined within the single or the multi-channel configuration. It cannot leave the system and, at the same time, there is not injection of external liquid or flow forcing. Numerical methods and detailed description of the CFD model employed here are provided in our previous publications [10–13].

3 Results and discussion

A certain number of simulations at $\mu_\ell = 1\text{–}3 \times 10^{-3}$ kg m^{-1} s^{-1}, $\mu_g = 8.76 \times 10^{-6}$ kg m^{-1} s^{-1}, $\rho_\ell = 1{,}000\text{–}1{,}500$ kg m^{-3}, $\rho_g = 0.07$ kg m^{-3}, $d = 10^{-5}\text{–}10^{-4}$ m, $z = 2$, $M = 2 \times 10^{-3}$ kg mol^{-1}, $i = 100\text{–}1{,}000$ A m^{-2}, and $h = 2\text{–}3 \times 10^{-3}$ m were run for both single and multi-channel systems (see Table 1). The values of the density and the viscosity of the liquid go from simple water to electrolyte-rich solutions in chlorate cells. Concerning the gas, only hydrogen was considered. According to the system investigated (multi- or single channel) and the values of current density i, bubble diameter d and channel thickness h, two (or three if we consider an intermediate transitional regime) different flow regimes are calculated (see also [10, 11]).

3.1 Quasi-steady regime

Under certain conditions (e.g. low current density and large bubble diameters) the flow shows a pattern, which was called in [10] as quasi-steady. Figure 2 (left) shows the velocity and void fraction profiles for the quasi-steady regime in a single channel configuration. The simulations were carried out at transient conditions, but the profiles reported in Fig. 2 remain almost constant during time, and for this reason this type of flow was called quasi-steady. The channel can be roughly divided in two regions: the bulk and the gas blanket. The gas blanket is where most of the gas is concentrated. In this region, the gas moves upwards due to buoyancy and the relatively small fraction of liquid follows the gas because of the drag force between the two phases. The bulk is the remaining part of the channel, where the void fraction is low. It also can be divided in two regions: the bulk upstream and the bulk downstream (Fig. 2). The bulk upstream is the region contiguous to the gas blanket. The momentum exchange between the gas blanket and the bulk upstream causes the latter to move upwards. Once the liquid flow reaches the top, the liquid must turn around the free surface because it cannot escape the channel. As a consequence, the flow in the left side of the channel must move downwards. This region is called bulk downstream. Most of the bubbles exit the gap from the top and, in fact, the void fraction in the bulk is lower. If the bubbles are small, however, the relative gas–liquid velocity is low and, as a consequence, some

Table 1 Cases simulated

Case	d [μm]	i [A m^{-2}]	h [mm]	μ_ℓ [kg m^{-1} s^{-1}]	ρ_ℓ [kg m^{-3}]
1	100	1,000	3	0.001	1,000
2	10	200	3	0.001	1,000
3	10	500	3	0.001	1,000
4	100	1,000	3	0.001	1,000
5	50	1,000	3	0.001	1,000
6	25	1,000	3	0.001	1,000
7	15	1,000	3	0.001	1,000
8	15	800	3	0.001	1,000
9	15	600	3	0.001	1,000
10	15	400	3	0.001	1,000
11	15	100	3	0.001	1,000
12	100	500	3	0.001	1,000
13	10	400	3	0.001	1,000
14	100	1,000	3	0.003	1,500
15	75	1,000	3	0.003	1,500
16	50	1,000	3	0.003	1,500
17	25	1,000	3	0.003	1,500
18	10	1,000	3	0.003	1,500
19	125	1,000	3	0.003	1,500
20	150	1,000	3	0.003	1,500
21	175	1,000	3	0.003	1,500
22	200	1,000	3	0.003	1,500
23	225	1,000	3	0.003	1,500
24	20	1,000	3	0.003	1,500
25	15	1,000	3	0.003	1,500
26	11	1,000	3	0.003	1,500
27	12	1,000	3	0.003	1,500
28	13	1,000	3	0.003	1,500
29	14	1,000	3	0.003	1,500
30	16	1,000	3	0.003	1,500
31	8	1,000	3	0.003	1,500
32	25	1,500	3	0.003	1,500
33	10	500	3	0.003	1,500
34	10	100	3	0.003	1,500
35	10	200	3	0.003	1,500
36	10	300	3	0.003	1,500
37	10	400	3	0.003	1,500
38	10	150	3	0.003	1,500
39	10	160	3	0.003	1,500
40	10	180	3	0.003	1,500
41	50	200	3	0.003	1,500
42	20	200	3	0.003	1,500
43	15	200	3	0.003	1,500
44	15	300	3	0.003	1,500
45	100	200	3	0.003	1,500
46	14	200	3	0.003	1,500
47	14	300	3	0.003	1,500
48	14	500	3	0.003	1,500
49	14	450	3	0.003	1,500
50	14	550	3	0.003	1,500
51	12	200	3	0.003	1,500
52	12	300	3	0.003	1,500
53	12	400	3	0.003	1,500
54	14	250	4	0.001	1,000
55	15	250	4	0.001	1,000
56	16	250	4	0.001	1,000
57	10	250	4	0.001	1,000
58	14	1,000	4	0.001	1,000
59	10	300	4	0.003	1,500
60	12	500	4	0.003	1,500
61	14	1,100	4	0.003	1,500
62	10	700	4	0.003	1,500
63	12	1,300	4	0.003	1,500
64	14	2,600	4	0.003	1,500
65	10	50	2	0.003	1,500
66	12	100	2	0.003	1,500
67	14	225	2	0.003	1,500
68	10	125	2	0.003	1,500
69	12	250	2	0.003	1,500
70	14	450	2	0.003	1,500

of the bubbles are not discharged from the top, but recirculate back with the liquid. The lower the diameter, the higher the fraction of bubbles dragged back into the bulk downstream by this mechanism (the same concept is also discussed later, at the end of Sect. 3 and in Fig. 6).

Simulations carried out with higher values of d confirm that the amount of gas recirculated in the bulk depends on the bubble size. Another parameter that, obviously, affects the void fraction in both the bulk and the gas blanket is the current density. If the current density is higher, more bubbles are produced and, consequently, more bubbles have the possibility to recirculate. Figure 2 (left) was calculated for the case of the single channel. The equivalent profiles for the multi-channel channel are reported in Fig. 2 (right). The velocity profiles are similar, but in the bulk region almost no trace of gas is detected. This depends on the fact that the free liquid surface is not immediately at the top of the channel, as in the previous case, but above the upper part, which connects all the three channels. The bulk velocity profile can still be divided in bulk upstream and bulk downstream, but the reasons of this, this time, does not depend directly on the liquid recirculation at the free surface. In this circumstance, the reason of the bulk downstream is that, since the gas is produced only on one side of the channel, there is an asymmetrical displacement

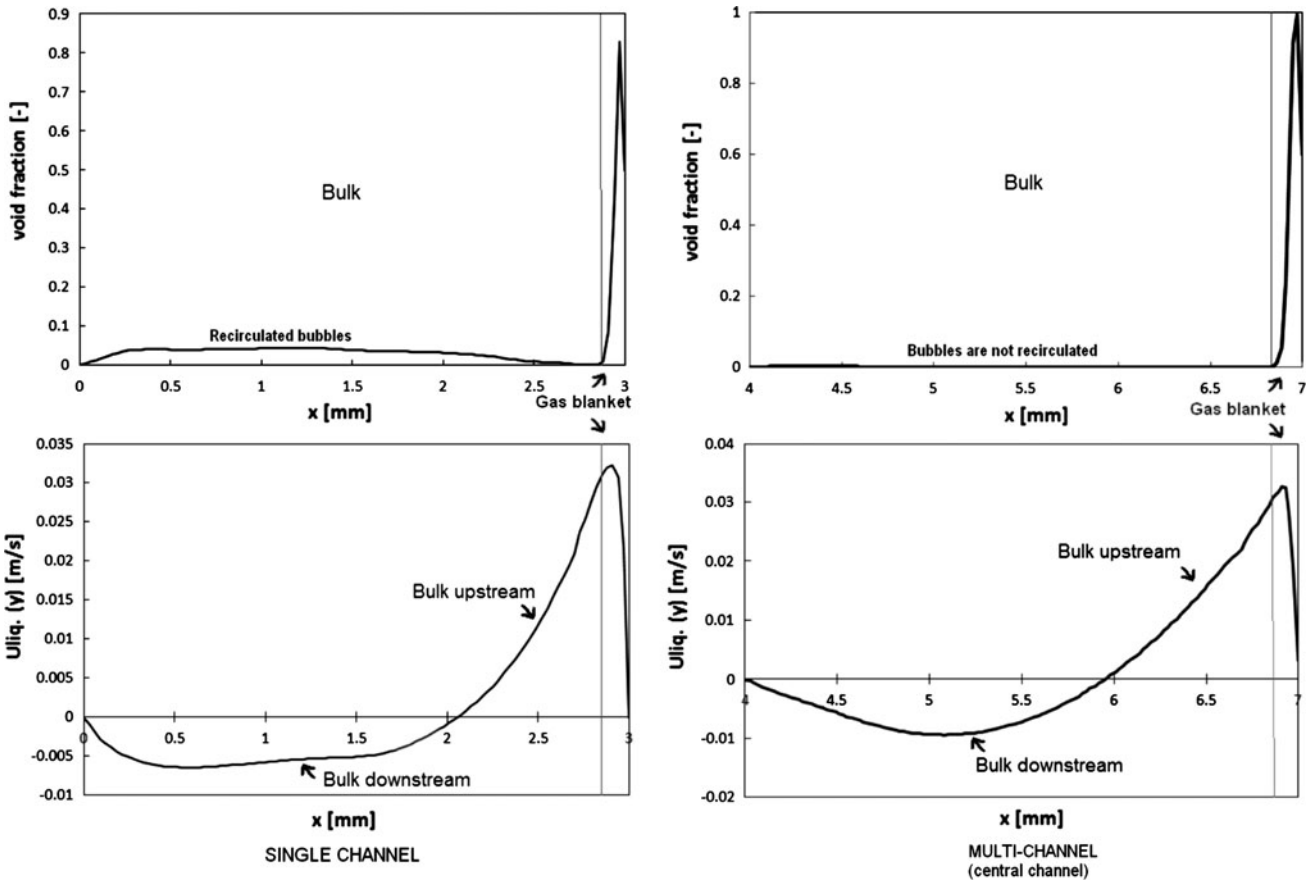

Fig. 2 Typical void fraction and velocity profiles (y component) in the single channel and in the central of the three channels configuration in the pseudo-turbulent regime ($i = 100$ A m^{-2}, $d = 0.01$ mm)

of the liquid, which can force downwards the flow in the region close to the opposite, non-gas-producing, electrode. As Fig. 3 indicates, in fact, the liquid recirculation in the case of the multi-channel system does not occur directly at the top of the channel, but in the region above it. This makes a big difference in the void fraction distribution. Since there is no liquid free surface at the top of the channel, the bubbles are free to move in the upper part of the system. Eventually, they can be partially recirculated in this region where the free liquid surface is located. For these reasons, while the velocity profiles between the single and multi-channel systems are similar for the quasi-steady regime, the void fraction in the bulk is different (Fig. 2).

3.2 Pseudo-turbulent regime

If, starting from the quasi-steady regime, we increase the current density i or we run the simulations with a lower value of the bubble diameter d, in the case of the single channel system, we initially observe the periodic formation of some burst of gas from the gas blanket to the bulk. These bursts temporarily modify the previously discussed void fraction and velocity profiles; however, if time average profiles are calculated, they do not differ considerably from the quasi-steady profiles. If, however, the current density is further increased or the bubble diameter further decreased, the frequency of these bursts increases. More and more gas is projected from the blanket to the bulk and, at a certain point, the velocity profile in the channel changes completely. Although the flow remains laminar [10], stable vortices and recirculation regions appear (see Fig. 4) and, for this reason, this type of regime was called pseudo-turbulent. These vortices increase the mixing in the channel, but at the same time, they also increase the average void fraction; many bubbles, in fact, are trapped in the vortices instead of being discharged at the top. The overall effect in terms of cell performance is still under study. On one hand, in fact, higher mixing is beneficial because it decreases concentration gradients at the electrodes. But, a higher void fraction, on the other hand, can be detrimental because it increases the overall electrical resistance of the cell. The conditions, which affect the transition from quasi-steady to quasi-turbulent regime, were investigated in [12]. The operative variables that were found to be responsible from the transition were i, d and h. Their effect was summarized by the following dimensionless group.

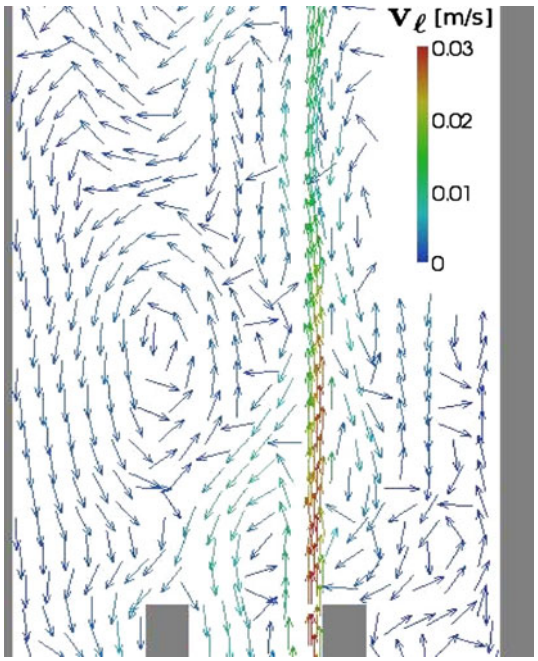

Fig. 3 Recirculation in the top region (*above the gaps*) of the multi-channel system

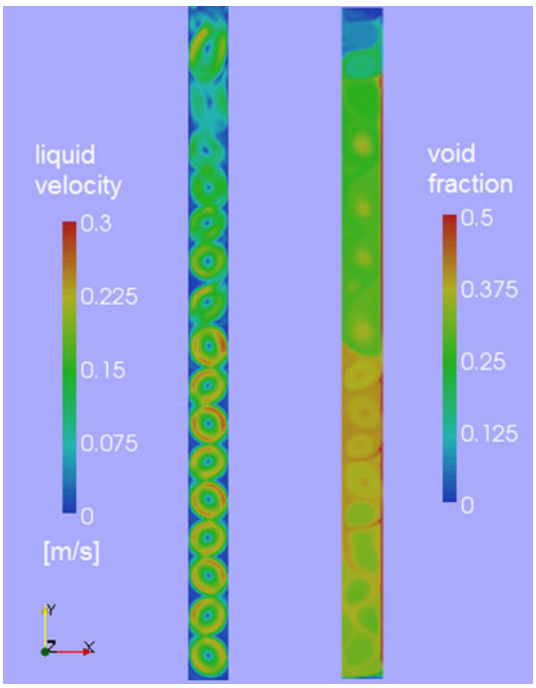

Fig. 4 Liquid velocity and void fraction in the quasi-turbulent regime (single channel)

$$\frac{j_{\text{gas}}(\mu_l/\rho_l)^{11/3}}{d^4h^2g^{7/3}} = K, \tag{3}$$

where the effect of the current density i is included in j_{gas} according to Eq. 1. If the value of K is less than 1.07×10^{-4}, the flow is in the quasi-steady regime, while if it is higher than 2.34×10^{-4}, the flow is in the pseudo-turbulent regime. If K is in between these two values, the flow is in an intermediate state where some vortices are detected in the channel; however, at the same time, they are not stable as in the case of the pseudo-turbulent regime. More details on the features and differences among these hydrodynamic regimes are given in [10].

The dimensionless group presented in Eq. 2 summarizes the results of our numerical simulations. If the current density i (or j_{gas} in Eq. 3) increases, the bubble diameter d decreases or the channel thickness h decreases, K increases and, therefore, the flow moves towards pseudo-turbulence. The transition, in particular, is particularly sensitive to the bubble diameter d, which appears in Eq. 2 raised to the fourth power.

So far, only the transition in the single channel was described. We could not find, however, pseudo-turbulence in the multi-channel system. The flow always remains in the quasi-steady regime (see also [11]). At very high values of i, which are not discussed here, transition to real turbulence occurs, but pseudo-turbulence was never detected. The reasons for this apparently paradoxical behaviour are described in the following section.

3.3 A closer look at the transition

Close observation of the behaviour of the bubbles in our simulations suggests the following mechanism for regime transition. In a single vertical channel, the liquid must turn around at the top because of the free surface. If the bubbles are large, they are most likely to reach a high relative velocity and escape the channel by disengaging at the top. If the bubbles are small, on the contrary, many of them are dragged back into the channel by the recirculating liquid. In the CFD simulations, we observe that, when the quantity of bubbles that are recirculated exceeds a certain value, the flow turns pseudo-turbulent. This phenomenon can be explained employing a more theoretical approach initially proposed in [12] to study the stability of the quasi-steady flow in a single channel. This approach was based on a simplified version of the flow where the velocity profile was assumed piecewise linear and the liquid pseudo-homogenous and inviscid. Figure 5 shows the simplified velocity profile adopted; the wall velocities are not zero because of the inviscid hypothesis. The system was divided in two parts, the gas blanket and the bulk. The gas blanket is entirely composed of gas. The bulk is a pseudo-homogenous mixture of gas and liquid. The key parameter, as illustrated later, is the density ratio q between the gas blanket and the bulk. If more gas reaches the bulk, q increases. Perturbative quantities of the type

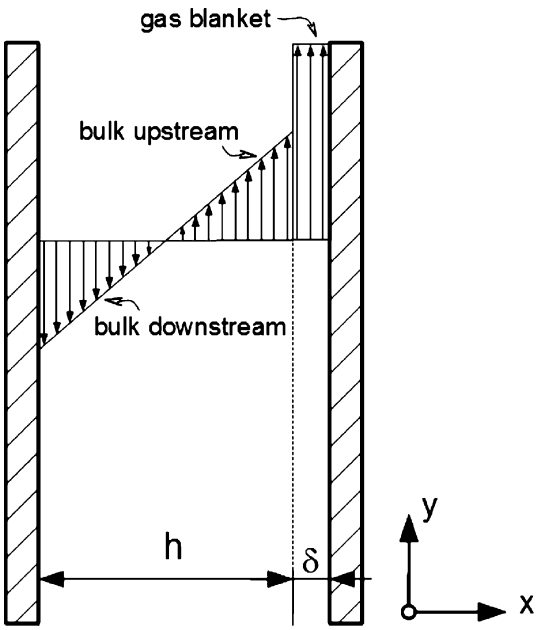

Fig. 5 Simplified flow in the channel

$$\mathbf{u}'(\mathbf{x},t) = \hat{u}(x)e^{j\kappa(y-ct)},\ p'(\mathbf{x},t) = \hat{p}(x)e^{j\kappa(y-ct)} \quad (4)$$

where j the imaginary unit, κ the wave number and c the wave speed of the disturbance were considered [12] and the simplified Navier–Stokes equations solved to determine the stability of the flow, which is stable if the imaginary part of c is positive, unstable otherwise. The results indicate that the stability depends on the density ratio q. If q increases above a critical value, the flow becomes instable. The critical value was found to be, in our case, around 10^{-3}, which means a void fraction in the bulk of about 0.1 and it is consistent with the CFD calculations. Owing to the simplifications adopted in the model, however, in this case we are not particularly interested in the numerical values, but mostly at the comparison of the trends obtained with the simplified and the CFD model.

The CFD simulations show that the transition to pseudo-turbulence is favoured by low bubble diameters d, high gas injections j_{gas} and small channel width h. All these observations are in line with the predictions of the above described inviscid model.

From the CFD simulations, for instance, we observe that the pseudo-turbulent regime appears only below a critical bubble diameter d_{cr}. We also see that if the bubble diameter d is small, the fraction of bubbles dragged back by the liquid recirculation increases and, therefore, the density in the bulk decreases. If the density in the bulk of our inviscid model is decreased, the density ratio between the gas blanket and the bulk is increased and the flow is more instable.

If the gas injection j_{gas} increases, the number of bubbles injected into the system is larger and, thus, a larger number of them are recirculated. In this way, the density of the bulk decreases, which, as already explained, leads to an increased region of instability.

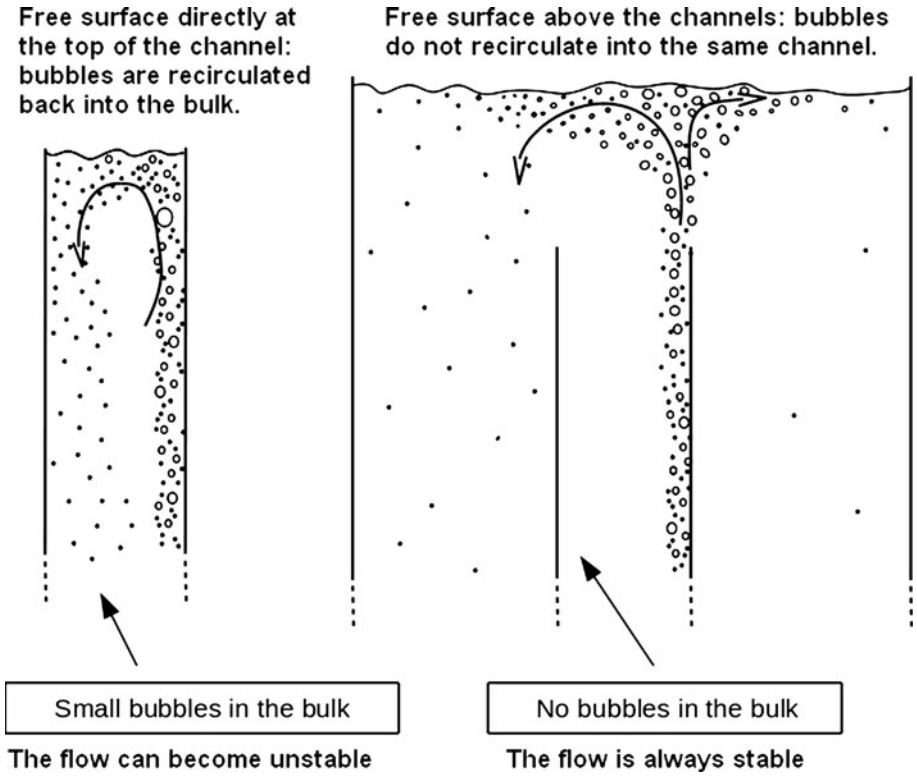

Fig. 6 Schematic recirculation of small bubbles in single channel (*left*) and multi-channel (*right*) systems

If the channel is narrower, the total mass of the liquid is smaller. Thus, the same number of recirculating bubbles has a higher impact on reducing the bulk density than in a wider channel. As a consequence, a smaller number of bubbles are sufficient to reduce the density in the bulk and thus increase the density ratio q in the inviscid model. Thus, the overall effect of a smaller channel width h based on our inviscid model is to destabilize the flow. This is also in line with Eq. 3. Such behaviour is indeed confirmed by the CFD calculations in the range investigated ($h =$ 2–4 mm). Usually a smaller channel thickness is suspected of stabilizing the flow because of the effect of viscosity, but this is not evident in our CFD computations. The fact that our pseudo-homogeneous inviscid model and our computational solution of the two-fluid model predict the same trends with respect to channel thickness, h, indicates that we were justified in considering an inviscid model for our preliminary stability analysis presented here.

In [12], the investigation was limited to the case of single channels, but we can here easily extend the discussion to the multiple-channel geometry. Following the previous reasoning, in fact, the different behaviour between the single and the multi-channel systems can be explained by the circumstance that, in the latter case, the free surface is not located immediately at the top of the channel, but in the connecting region above. As a consequence, more gas disengagement happens above the channel walls, the liquid recirculation occurs in the upper region and the small bubbles are not dragged back into the bulk of the channel (see Fig. 6). According to our stability criterion, therefore, the transition to pseudo-turbulence cannot occur in the multi-channel geometry: the data obtained with the CFD model completely confirm this result.

4 Conclusions

In the last years, CFD has been extensively used by both our [10–13] and other (e.g. [2–9]) research groups for simulating the flow in electrochemical systems of industrial interest. These works provided fundamental insights into the hydrodynamic phenomena occurring in electrochemical reactors, but they also raised some important questions that have never been answered so far. One of these questions concerns the apparently paradoxical difference between single and multi-channel geometries initially observed in [11]. Here, the findings of [11] are observed under a new light by means of the method initially, developed in [12], for analysing the stability of the flows in single channel systems. This approach allows us to relate the stability of the flow and, therefore, its hydrodynamics to the void fraction in the bulk of the channel. In this way, the stable hydrodynamics observed in multi-channel systems can be explained by the lack of bubble recirculation at the top of the channels. This result can open the way to a new method of controlling the mixing in electrochemical multi-channel reactors with gas evolution at the electrodes. According to the theory develop in this study, in fact, it would be possible to increase or decrease the mixing of the system by, respectively, allowing or preventing small bubbles from reaching the bulk of the channels.

Appendix: Two phase flow

The velocity field is computed by solving the continuity and Navier–Stokes equations for a biphasic flow consisting of a dispersed and continuous phase according to the so-called Euler–Euler model. In this approach, both the continuous and dispersed phases are considered to be interpenetrating continua and the macroscopic description of both phases is derived by averaging the conservation equations for each phase.

Dispersed phase

$$\frac{\partial \alpha \rho_g}{\partial t} + \nabla \cdot \left(\alpha \rho_g \mathbf{v}_g\right) = 0, \tag{5}$$

$$\frac{\partial \alpha \rho_g \mathbf{v}_g}{\partial t} + \mathbf{v}_g \cdot \nabla\left(\alpha \rho_g \mathbf{v}_g\right) = \alpha\left(\mathbf{g}\rho_g - \nabla p\right) + \nabla \cdot \left[\alpha \mu_g \left(\nabla \mathbf{v}_g + \nabla \mathbf{v}_g^T\right)\right] - \mathbf{M}, \tag{6}$$

Continuous phase

$$\frac{\partial (1-\alpha)\rho_\ell}{\partial t} + \nabla \cdot \left((1-\alpha)\rho_\ell \mathbf{v}_\ell\right) = 0, \tag{7}$$

$$\frac{\partial (1-\alpha)\rho_\ell \mathbf{v}_\ell}{\partial t} + \mathbf{v}_\ell \cdot \nabla \mathbf{v}_\ell [(1-\alpha)\rho_\ell] = (1-\alpha)(\mathbf{g}\rho_\ell - \nabla p) + \nabla \cdot \left[(1-\alpha)\mu_\ell \left(\nabla \mathbf{v}_\ell + \nabla \mathbf{v}_\ell^T\right)\right] + \mathbf{M}. \tag{8}$$

The last term M in Eqs. 6 and 8 represents the interfacial momentum transfer, which is usually divided into several different parts each contributing drag, lift, virtual mass forces, interfacial pressure, etc. In our case, only drag is considered (Wen and Yu model [30]). The effect of the lift force was evaluated [10] and resulted in little or no difference in the flow pattern. The possible presence of a slip velocity at the cathode has been discussed in [13]. The mesh used is a structured rectangular mesh. It was found [10] that a mesh with a characteristic size of

0.1 × 0.1 mm, except for the last three cells close to the electrode, which are further divided into 15 smaller cells, is appropriate. Grid independence of the results was checked [10]. The time steps were assumed variable to assure a maximum Courant number smaller than 0.5. The overall simulated time was 80 s for both configurations. Time averages were computed considering times from 40 to 80 s, after verifying that steady state (in statistical sense) is reached. As already stated, all the physical properties (gas and liquid densities and viscosities, bubble size, etc.), operational variables (current density, wall void fraction, etc.) and numerical parameters (mesh structure and characteristic size, strategy for determining the variable time step, etc.) are the same in the two cases. The only significant difference is, therefore, the presence of only one gap instead of three and the presence of the external reactor volume.

References

1. Vogt H (1983) Comprehensive treatise of electrochemistry, vol 6. Plenum Press, New York
2. Aldas K, Pehlivanoglu N, Mat MD (2008) Int J Hydrogen Energy 33:3668
3. Byrne P, Fontes E, Parhammar O, Lindbergh G (2001) J Electrochem Soc 148:125
4. Gurniki F, Bark F, Zahrai S (1999) J Appl Electrochem 29:27
5. Gurniki F, Fukagata K, Zahrai S, Bark F (2000) J Appl Electrochem 30:1335
6. Mat MD, Aldas K (2005) Int J Hydrogen Energy 30:411
7. Mat MD, Aldas K, Ilegbusi OJ (2004) Int J Hydrogen Energy 29:1015
8. Cavalcanti RD, Neto SRD, Vilar EOA (2005) Braz Arch Biol Technol 48:219
9. Wedin R, Dahlkild A (2001) Ind Eng Chem Res 40: 5228
10. Alexiadis A, Dudukovic MP, Ramachandran P, Cornell A, Wanngård J, Bokkers A (2011) Chem Eng Sci 66:2252
11. Alexiadis A, Dudukovic MP, Ramachandran P, Cornell A, Wanngård J, Bokkers A (2012) The flow pattern in single and multiple submerged channels with gas evolution at the electrodes. Int J Chem Eng 2012(2012):9
12. Alexiadis A, Dudukovic MP, Ramachandran P, Cornell A, Wanngård J, Bokkers A (2011) Theor Comput Fluid Dyn (article in press, available on-line at http://www.springerlink.com/content/f3623j5334130858/). Accessed 07 May 2012
13. Alexiadis A, Dudukovic MP, Ramachandran P, Cornell A, Wanngård J, Bokkers A (2011) Int J Hydrogen Energy 36:8857
14. Vogt H (1984) Electrochim Acta 29:167
15. Vogt H (1984) Electrochim Acta 29:175
16. Boissonneau P, Byrne (2000) J Appl Electrochem 30:767
17. EI-Shakre ME, Saleh MM, EI-Anadouli BE, Ateya BG (1994) J Electrochem Soc 141:441
18. Caire JP, Espinasse G, Dupoizat M, Peyrard M (2009) WIT Trans Eng Sci 65:23
19. Roustan H, Caire JP, Nicolas F, Pham P (1998) J Appl Electrochem 28:237
20. Petersen MA, Reardon KF (2009) AIChE 55:2468
21. Nierhaus T, Van Parys H, Dehaeck S, van Beeck J, Deconinck H, Deconinck J, Hubinc A (2009) J Electrochem Soc 156:139
22. Tomasoni F, Thomas JF, Yildiz D, van Beeck J, Deconinck J (2007) WIT Trans Eng Sci 54:153
23. Alexiadis A, Cornell A, Dudukovic MP (2012) Comparison between CFD calculations of the flow in a rotating disk cell and the Cochran/Levich equations. J Electroanal Chem 669:55
24. Ashraf Ali B, Pushpavanam S (2011) Int J Multiph Flow 37:1191
25. Nierhaus T, Vanden Abeele D, Deconinck H (2007) Int J Heat Fluid Flow 28:542
26. Van Damme S, Maciel P, Van Parys H, Deconinck J, Hubin A, Deconinck H (2010) Electrochem Commun 12:664
27. Van Parys H, Van Damme S, Maciel P, Nierhaus T, Tomasoni F, Hubin A, Deconinck H, Deconinck J (2009) WIT Trans Eng Sci 65:109
28. Maciel P, Nierhaus T, Van Damme S, Van Parys H, Deconinck J, Hubin A (2009) Electrochem Commun 11:875
29. Mandin P, Roustan H, Wüthrich R, Hamburger J, Picard G (2007) WIT Trans Eng Sci 54:73
30. Wen CY, Yu YH (1966) Chem Eng Prog Symp Ser 62:100